INTERNATIONAL REVIEWS IN PHYSICAL CHEMISTRY, 1998, VOL. 17, NO. 4, 525–546

Quantum modelling of reactions in solution: an overview of the dielectric continuum methodology

THANH N. TRUONG

Henry Eyring Center for Theoretical Chemistry, Department of Chemistry, University of Utah, Salt Lake City, Utah 84112, USA

In this review, we report on the status and perspectives for theoretical modelling of solvent effects on reactions in solution using quantum-mechanical methods coupled with the dielectric continuum solvation methodology. The simplicity of the dielectric continuum approach allows inclusion of solvent effects directly into the solute Hamiltonian. Thus, it provides a practical tool for optimizing transition state structures and following reaction paths of reactions in solution in a rather routine manner as for gas-phase systems. Several different types of reaction are examined in more details to illustrate the advantages and disadvantages, accuracy and applicability of the continuum models employed.

1. Introduction

Since the beginning of this decade, there have been significant efforts devoted towards the development of methodology in quantum chemistry for understanding solvent effects. Considerable progress has been achieved although many challenges still remain. In this review, I shall particularly focus on developments of the dielectric continuum approach. Several excellent reviews have been published recently in this subject with attention given to the accuracy of different continuum models in calculating the free energy of solvation, equilibrium and spectroscopic properties of molecules in solution [1–3]. The present paper offers a different view and focuses on an area that has not been emphasized in previous reviews. Specifically, the emphasis of this review is not on the theoretical models but on interesting and important chemical properties, namely solvent effects on the transition states and free-energy profiles of reactions in solution while asking several questions as follows. Is the dielectric continuum approach an appropriate methodology? What are its advantages and disadvantages compared with other existing methodologies? Is the dielectric continuum methodology at the stage where an accurate transition state and free-energy profile can be calculated as routinely as for the gas-phase systems?

Transition states and free-energy profiles are important for elucidating mechanisms of reactions in solution and are the starting point for addressing their dynamics. Despite their importance, modelling these properties for reactions in solution has been a challenge in quantum chemistry. The challenge arises from the two requirements that adequate theoretical models must have an accurate description of both the variation in the electronic structure of the system as it proceeds from the reactants to products and the solvent–solute interactions. The first requirement demands accurate correlated level of *ab initio* molecular orbital (MO) or non-local density functional theory (DFT). For solvent–solute interactions, several reasonably accurate models exist in the literature. Generally these models can be classified into two groups: one treats the solvent explicitly, and the other implicitly. I provide here a brief overview of different models and proceed directly to a discussion of how they are employed in studying reaction mechanisms.

0144–235X/98 $12.00

2. Solvation models

Within the explicit treatment approach, there are two general methodologies. The supermolecule model [4] treats a small number of first-solvation-shell solvent molecules explicitly at the same quantum-mechanical (QM) level as the solute. This model offers a straightforward and accurate way to account for the localized portion of the solvent–solute interactions. In applications, it is the method of choice for studying bifunctional properties of polar solvents and microsolvation. For instance, in water-assisted tautomerization or proton transfer processes, solvent waters can directly participate in the chemical reaction [5, 6]. Such waters much be treated quantum-mechanically. In microsolvation, studying hydrated clusters often provides essential microscopic features of solvent effects on chemical reactions [7–10]. A major drawback is that this model cannot include the long-range electrostatic interactions with the bulk solvent. With recent advances in computer technology, quantum simulations of equilibrium properties of condensed-phase systems with inclusion of long-range solvent–solute interactions is now possible with the use of the Car–Parrinello approach [11–13]. However, such calculations are still computationally expensive. A common methodology is to construct an approximate solvent–solute interaction potential for use in simulations of condensed-phase properties. The simplest form of such a potential is the use of classical molecular mechanics (MM) force fields [14]. With increasing complexity and accuracy, the empirical valence bond method [15], the combined QM–MM method [16–19] and the effective fragment method [20] allow for a small but important part of the system such as solutes to be treated quantum-mechanically while the remaining is represented classically. Finally, the frozen (or embedded) DFT [21, 22] treats solvent molecules as frozen density objects. This is perhaps the closest approximation to the full QM treatment. Long-range interactions with the bulk solvent can be included by using the periodic boundary condition with a sufficiently large unit cell. For thermodynamic condensed-phase properties, large molecular dynamics (MD) or Monte Carlo (MC) simulations can be carried out to sample over both solute and solvent configuration space. Alternatively, a less computationally demanding integral equation approach such as the extended reference interaction site method (RISM) [23, 24] can be used.

There are several methodologies for implicit treatment of the solvent, such as Langevin dipole and dielectric continuum models. Among these existing solvent models, the dielectric continuum approach offers the simplest and yet reasonably accurate methodology. We shall limit our discussion of the implicit treatment of solvent to the dielectric continuum approach while referring readers elsewhere [25] for a detailed discussion of other models. In the dielectric continuum approach, the solvated system is modelled as the solute (if necessary, with inclusion of several first-solvation-shell solvent molecules) inside a cavity surrounded by a dielectric continuum medium represented by the dielectric constant ε. Most efforts in calculating solvent–solute interactions so far have been focused on the electrostatic nature which is the major contribution in polar solvents. More attention is now turning toward the non-electrostatic terms such as dispersion, repulsion and cavitation since they are becoming more important as the solvent polarity decreases. For electrostatic interactions, several methodologies exist such as the multipole expansion, image charge, apparent surface charge approaches or the finite-difference Poisson–Boltzmann method (see the review by Tomasi and Persico [2] for more details). Earlier solvation models require the cavity to have spherical or ellipsoidal shape while more recent ones can treat arbitrary shape cavities. It has been known that models based on

molecular-shape cavities can lead to more accurate descriptions of the solvent–solute interactions. Several such models exist and have shown some promise for studying reactions in solution due to the availability of analytical free-energy derivatives. They are the polarizable continuum model (PCM) [2, 26–29], the reaction field factors formalism [30, 31], which is based on the Kirkwood multipole expansion model [32], the Poisson–Boltzmann method [33, 34], the conductor-like screening model (COSMO) method [35] implemented at the DFT [36] or *ab initio* MO theory [37] and its generalization, the generalized conductor-like screening model (GCOSMO) [38, 39]. Several reviews [1–3] have provided excellent discussions and analyses of these methodologies.

3. Challenges in modelling transition states and reaction profiles in solution

For reaction in the gas phase, there is a simple and straightforward procedure for calculating the transition-state structure and reaction path. First, one searches for the transition state which is a local saddle point on the potential energy surface. One then performs a normal mode analysis to verify whether it is the correct transition state by having only one imaginary frequency whose eigenvector corresponds to the direction of the reaction. Subsequently, one can determine the minimum-energy path by following the steepest-descent path that connects the transition state to the reactants and products to provide additional information on structural variations along the reaction coordinate and the shape of the potential curve. To elucidate the reaction mechanism, it is often sufficient to have only structural, energy and frequency information at the stationary points, that is reactants, transition state and products.

In solution, there is no such straightforward recipe. The procedure depends on how one models the solvent. For the explicit solvent treatment, the large number of solvent degrees of freedom prevents one from uniquely defining the transition state, the minimum-energy path (MEP) and thus the reaction coordinate. This is perhaps the greatest challenge for the explicit solvent methodology. Consequently, this approach mostly relies on the gas phase or a simple user-defined reaction coordinate. Hence, participation of solvent motions in the reaction coordinate is ignored. Such practice works reasonably well for many simple reactions. For complex reactions where competing reaction paths exist and where solvent effects drastically change the topology of the free-energy surface, one is required to examine all possible free-energy pathways but this would be too costly. Since the transition state is not well defined within this approach, to elucidate the reaction mechanism one is required to determine the whole potential of mean force along the reaction coordinate using a standard statistical mechanics technique such as the thermodynamic integration or free-energy perturbation method. However, such calculations require a large number of free-energy simulations, typically around 30–60 runs. This is not only a tedious task but also quite time consuming and computationally expensive. The extended RISM provides a more efficient tool to obtain the free-energy profiles by solving for radial distribution functions [40]. However, it relinquishes most of the detailed microscopic structural information.

The dielectric continuum approach, however, does not have the above difficulties since solvent effects are effectively included in the solute Hamiltonian and do not increase the dimensionality of the system. The 'effective' transition state and minimum free-energy path (MFEP) can be uniquely defined similar to those of the gas-phase system. Furthermore, availability of analytical free-energy derivatives greatly

enhances the ability to explore the free-energy surface and to characterize stationary points. These advantages, of course, do not come without a cost. This approach forfeits detailed solvent structure for computational simplicity. Furthermore, the uncertainty in specification of the location of the boundary between atomistic and continuum descriptions of the system reduces the confidence level on the accuracy of the calculated results. It is also worth noting that, since a solvent is treated as a uniform dielectric medium, this approach does not include specific hydrogen bond effects. In principle, one can account for these effects by including several important first-solvation-shell solvent molecules in the cavity. However, in this case statistical averaging over all explicit solvent degrees of freedom is required in order to calculate thermodynamic quantities.

Finally, it is possible to combine the advantages of both explicit and implicit solvent approaches. Lim and Jorgensen [41] recently proposed such a combined approach where dielectric continuum models are used to determine transition-state structures in solution, and then MC free-energy perturbation simulations are employed to provide accurate changes in the activation energy upon transferring to different solvents and detailed solvent structural information.

4. Progress in applications

The dielectric continuum methodology has been employed in theoretical studies of solvent effects on mechanisms of various reactions, such as S_N2 charge transfer [42–53], proton transfer [10, 54–58], cycloaddition [41, 59–74], nuclear addition [6, 75–80], Diels–Alder [81–88], rearrangement [89–96] and isomerization [92, 97–102] reactions. From a theoretical point of view, these studies share two general features. First, most of them have employed the self-consistent reaction field (SCRF) model [103] using a simple (spherical or ellipsoidal) cavity. Second, many involved only geometry optimizations of stationary points. Free-energy profiles were not calculated. Several studies have estimated the MFEP either from the reduced two-dimensional (2D) free-energy surfaces, or by adding solvation free energies to the potential energy along the gas-phase MEP or along a user-defined reaction coordinate. Below I provide an overview on the progress on applications of the dielectric continuum approach to elucidate reaction mechanisms. However, I shall limit the discussion to several particular types of reaction that have attracted numerous theoretical studies owing to their interesting and significant solvent effects, namely the S_N2 charge-transfer, the polar cycloaddition, the Diels–Alder and the Claisen rearrangement reactions.

4.1. *S_N2 charge-transfer reactions*

There are two types of S_N2 reaction. Type I reactions are charge-transfer processes, such as the symmetric charge-transfer $Cl^- + CH_3Cl$ reaction while type II reactions are charge separation processes such as the Menshutkin $NH_3 + CH_3Cl \rightarrow H_3NCH_3^+ + Cl^-$ reaction. Type I S_N2 reactions have been widely studied both theoretically and experimentally owing to their important role in physical organic chemistry and to their large solvent effects [104–108]. For instance, for the $Cl^- + CH_3Cl$ reaction, aqueous solvent effects significantly decrease the reaction rate by 20 orders of magnitude owing to charge delocalization which leads to a decrease in the free energy of solvation at the transition state relative to the separated products. Although the reaction profile of the S_N2 reaction has a double-well form in the gas phase [109], it is believed to be unimodal in an aqueous environment [110]. Such important differences in the reaction profiles in

the vacuo and in solution were reproduced first by MC simulations [111], and then by MD simulations using different solvent–solute interaction models [112–115], and extended RISM integral equation [40] calculations with equal success. *Ab initio* studies [7, 8, 116] on hydrated clusters provided only qualitative features of the solvent effects. The accuracy of different dielectric continuum models in calculations of the reaction profile for this reaction was first examined by Alemán *et al.* [46]. These workers pointed out the advantages of the PCM model. Similar results were also obtained with more recent generalized Born [47, 48, 51] and GCOSMO [52] models. It is important to point out that, in previous GCOSMO calculations, the calculated gas-phase barrier is in excellent agreement with experimental derived data; however, the calculated free energy of activation for the reaction in water is underestimated by 7 kcal mol^{-1} compared with the experimental data of about 26 kcal mol^{-1}. This error was attributed to the uncertainty in the cavity size. As discussed in more detail below, it is actually due to omitting the contribution from the solute internal degrees of freedom.

The type II S_NS reactions differ from the type I S_N2 charge-transfer reactions, such as $Cl^- + CH_3Cl \rightarrow ClCH_3 + Cl^-$, in several aspects. First, the rate of the Menshutkin reaction has been found to increase dramatically with increasing solvent polarity instead of decreasing as in type I S_N2 reactions. Thus, polar solvents favour the charge separation process and stabilize the transition state. Second, the $Cl^- + CH_3Cl \rightarrow ClCH_3 + Cl^-$ reaction is symmetric; thus one expects very little solvent effect on the transition-state structure. In contrast, the Menshutkin reaction such as the $NH_3 + CH_3Cl \rightarrow H_3NCH_3^+ + Cl^-$ reaction is an asymmetric charge seperation process with an endothermicity of 110 kcal mol^{-1} in the gas phase but it is exothermic by about 34 ± 10 kcal mol^{-1} in aqueous solution owing to the stabilization of the $H_3CNH_3^+$ and Cl^- ions by the solvent [117]. According to the Hammond postulate [118], solvent effects would shift the transition state towards the reactant channel; thus the solvent has a direct participation in the reaction coordinate. This role of the solvent challenges the validity of the static equilibrium solvation treatment which assumes the solvent to be in equilibrium with the chemical system at each point along the gas-phase reaction coordinate. For this reason, this reaction provides a much more challenging test to any solvation theory attempting to model solvent effects on transition state structure and reaction profile. Gao and Xia [117] have performed elaborate MC simulations using an AM1–MM potential to map out a 2D free-energy surface for this reaction. The transition-state structure and the MFEP were then estimated from this 2D surface. Although these workers used a rather approximate AM1 Hamiltonian for the solute, their QM–MM description of solvent–solute interactions was quite accurate and the AM1 barrier height happened to agree well with the free energy of activation for the gas-phase reaction. They found a significant shift of the transition state towards the reactant channel and the free energy of activation to be 26.3 kcal mol^{-1} [117]. PCM dielectric continuum calculations done by Solà *et al.* [119] for the $NH_3 + CH_3Br$ reaction in water yielded an activation energy of only 8.3 kcal mol^{-1}. This value appears to be too low. This is mainly due to not including the contribution from the solute internal motions as discussed below. For the $NH_3 + CH_3Cl$ reaction, this contribution increases the free energy of activation by 13.1 kcal mol^{-1}. Using the reaction field factor continuum model, Dillet *et al.* [49] were able to optimize fully the transition state in solution and provided more detailed discussion on solvent effects on the transition-state structure. Full determination of the MFEP was done more recently with the use of the GCOSMO model [53]. Results from both models show excellent agreement with those from MC simulations. The agreement between results from

GCOSMO and reaction field factor calculations and AM1–MM simulations leads to an important conclusion that the electrostatic solvent–solute interaction makes the major contribution to the transition-state stabilization in type II S_N2 reactions and not the specific hydrogen bond interaction (as inferred by Gao and Xia).

4.2. *Cycloaddition reactions*

[2+2] cycloaddition reactions are useful synthetic routes to formation of four-membered rings. From the Woodward–Hoffmann rules, the [2+2] reactions are thermally allowed via a supra-antara transition state. These reactions are often classified into two classes, namely non-polar or polar cycloadditions, having rather different mechanisms. Stereochemical and kinetic data indicate that non-polar cycloadditions proceed via a two-step biradical mechanism with rather a large activation energy. On the contrary, polar cycloadditions in solution have much lower activation energies and were suggested to have a two-step mechanism with a zwitterionic intermediate [120, 121]. Dielectric continuum models have been used to investigate roles of solvents on the mechanisms of various polar cycloaddition reactions [41, 59–74]. Generally, polar solvents were found to stabilize the zwitterionic intermediate and consequently to alter the mechanism from a concerted process in the gas phase to a stepwise process in solution via a stable zwitterionic intermediate. This is qualitatively in accord with experimental observations. However, the magnitude of solvent effects on the free energy of activation was rather overestimated in a recent detailed analysis by Lim and Jorgensen [41] in comparisons with experimental data. For instance, the SCRF model and the PCM based on isodensity surface cavity calculations predict that the solvent effects lower the activation energy of the cycloaddition of 1,1-dicyanoethylene and methyl vinyl ether by 10–13 kcal mol^{-1} on going from CCl_4 to CH_3CN while the observed value is about 5 kcal mol^{-1}. Lim and Jorgensen have also performed elaborate MC simulations using the free-energy perturbation theory with an accurate force field that includes solute polarization effects and found much larger solvent effects of 18–20 kcal mol^{-1} on the activation energy. However, in our study [122] of the [2+2] cycloaddition of ketene and imine, the GCOSMO model predicts that the solvent lowers the activation energy by 4.5 kcal mol^{-1} on going from vacuum to water ($\varepsilon = 78.4$) while previous SCRF calculations [59, 60, 70] yield a value of 8.2 kcal mol^{-1} going from vacuum to CH_3CN ($\varepsilon = 37.5$). GCOSMO results, however, for different reactants fall within the range of experimental findings, thus supporting the use of a more accurate cavity representation.

4.3. *Diels–Alder reactions*

Solvent effects on Diels–Alder reactions have become an important topic for theoretical investigations owing to the observed significant rate enhancement with the use of aqueous solvent [123]. Furthermore, the endo–exo and diastereofacial selectivities were found to correlate well with solvent polarities, indicating that electrostatic solvent effects are important [82]. On the other hand, para–meta regioselectivities, diastereofacial selectivities and rate variation correlate well with hydrogen bond donor ability of the solvent [82].

Previous results from MC simulations [124] indicated that the rate accelation in water results mainly from hydrophobic and hydrogen bonding effects. Thus, in order to model correctly the solvent effects in Diels–Alder reactions, solvation models must include not only electrostatic but also solvophobic and hydrogen bond effect contributions. QM studies to date provide only qualitative trends. In fact, SCRF

calculations [81–83, 85, 86] show that electrostatic solvent effects slightly increase the activation barriers, that is in the opposite direction from experimental observation. Despite this fact, this simple continuum model was able to reproduce experimental trends on the endo–exo, para–meta and diastereofacial selectivities as functions of solvent polarity. These studies [81–83, 85, 86] also showed large effects on the geometry of the transition state and on the reaction path due to solvent polarization. In particular, an aqueous solvent promotes asynchronicity in the reaction coordinate, thus supporting the need for inclusion of solvent effects in the determination of the reaction path. Using the semiempirical generalized Born AM1–SM2 solvation model, the correct experimental trend was obtained; however, the calculated rate acceleration factor is smaller than results from MC simulations [125]. Since the SM2 solvation model [126] includes hydrophobic and specific hydrogen bonding effects, one can expect that it performs better than the SCRF model on the rate enhancement factor.

Supermolecule calculations [83] have also been carried out for a series of Diels–Alder reactions and found that they can account for the influence of hydrogen bond effects on endo–exo selectivities and activation energy experimentally observed. However, results on the para–meta regioselectivities for hydrated clusters are almost the same as for isolated molecules. This is not consistent with the experimental observation that, for strong hydrogen bonding donor solvents, such as fluorinated alcohols, the para-to-meta ratios significantly increase. However, such increases were not observed for reactions in water–alcohol mixtures. The supermolecule results were attributed to the inability of water to model strong hydrogen bond effects in fluorinated alcohols.

4.4. *Claisen rearrangement reactions*

The Claisen rearrangement, that is the thermally induced 3,3-sigmatropic shift of allyl vinyl eithers to γ,δ-unsaturated carbonyl compounds, has received much attention both experimentally and theoretically [127]. This is an important reaction in synthetic organic chemistry and has been used as a prototype in modelling the mechanism of the biosynthesis of phenylalanine. Similar to the Diels–Alder reactions, the Claisen rearrangement was found experimentally to have a significant rate acceleration going from non-polar to polar solvents, and in particular a 214-fold increase from cyclohexane to aqueous solution, corresponding to a 3.2 kcal mol^{-1} decrease in the activation energy. This may first suggest that solvent polarization is responsible for such rate enhancement. However, the observed sevenfold increase in the rate in water relative to that in 2,2,2-trifluoroethanol (TFE) solvent does not support the importance of solvent dielectric effects since both water and TFE solvents have similar dielectric constants [127]. These later results suggest that specific hydrogen bonding effects are the major factor since TFE is a better hydrogen bond donor than water. This, however, contradicts the observed lack of a correlation between the rate effects with the acid dissociation constants of solvents [128]. For example, aqueous ethanol promotes the reaction to the same extent as phenol while the rate in octanoic acid is a factor of 2.8 times slower than in *p*-chlorophenol. Thus, specific hydrogen bond effects alone cannot explain the overall solvent effects in this reaction. This leads to the suggestion that hydrophobic effects also play a non-negligible role. Furthermore, the secondary deuterium kinetic isotope effects were found to be unaffected by the solvent polarity, indicating a little change on the transition-state structure for the reaction going from non-polar solvent to aqueous solution [127].

Theoretical studies [93–95, 129–132] to date are not conclusive on what components of the solvent–solute interactions govern the observed rate acceleration. Early MC simulations by Severance and Jorgensen [131] using an MM force field led to the conclusion that the increase in the hydrogen bonding at the transition state relative to the reactant is responsible for the calculated decrease in activation energy of 3.85 kcal mol^{-1} for the reaction in water compared with the gas phase. Including solute polarization in an AM1–MM potential for MC simulations, Sehgal *et al.* [130] concluded that a charge increase on the oxygen atom is the main factor in the rate acceleration corresponding to a decrease in the activation energy of 3.5 kcal mol^{-1} at 25 °C. SCRF calculations [93], which account only for the electrostatic component of the solvent–solute interaction, predict either a lowering of only 1.2 kcal mol^{-1}, or an increase of 1.1 kcal mol^{-1} in the activation energy depending on the method of including correlation effects, DFT or MP2 respectively. Using the SCRF, PCM and supermolecule models at different levels of theory, Davidson *et al.* [94, 95] found that the PCM, which includes dispersion, repulsion and cavitation contributions, yields a barrier lowering in water of 2.8 kcal mol^{-1}. The SCRF model yields a value of 0.7 kcal mol^{-1}, and the supermolecule approach with two explicit water molecules yields 5.2 kcal mol^{-1}. The latest non-local B3LYP DFT calculations [129] using the discrete-continuum approach, which models the system as the solute and two explicit solvent water molecules near the solute oxygen atom in a molecule-shaped cavity immersed in a dielectric medium, predict a decrease in the activation energy of 6.3 kcal mol^{-1}. Results from this model suggested that charge transfer to the first-solvation-shell solvent is an important factor for the rate acceleration. With the AM1–SM2 generalized Born continuum model, Storer *et al.* [132] concluded that electrostatic polarization and first-hydration-shell hydrophobic effects are the main factors accounting for the decrease of 4.3 kcal mol^{-1} in the activation energy. The results also indicated that hydrophobic packing effects are unimportant.

From the latest study by Guest *et al.* [129], solvent polarization described by the SCRF model and PCM were found to have large effects on the transition-state structure, that is both predict increased bond breaking and reduced bond formation upon hydration (increases in the bond distance of both the breaking and the forming bonds). Supermolecule calculations predict even larger effects. Finally, none of the solvation models predicts changes in the kinetic isotope effects upon going from non-polar to polar solvent in agreement with experimental observations.

5. Recent developments

Recently, a new methodology for calculating the MFEP using the dielectric continuum approach has been proposed [53]. This methodology provides a routine procedure for quantitative *ab initio* calculations of free energies of activation of reactions in solution. An overview of this general methodology is given below. This methodology can be used with any dielectric continuum model which has analytical free-energy derivatives. Two well studied examples are presented to illustrate the usage of this methodology. Since these illustrative examples use the GCOSMO model, the description of this model is also given.

5.1. *General methodology*

Let us consider an A → B reaction. The standard free energies of reaction in the gas phase and in solution are denoted as ΔG_g^0 and ΔG_s^0 respectively. Associated with the

reactant A and product B are free energies of solvation denoted as ΔG^0_{solv}. From the thermodynamic cycle given by

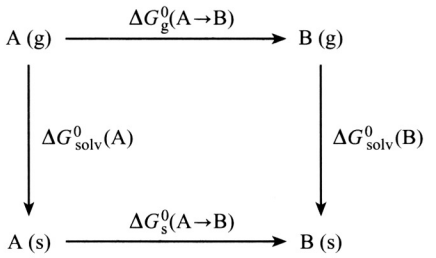

the standard free energy of the reaction in solution can be written as

$$\Delta G^0_s = \Delta G^0_g + [\Delta G^0_{\text{solv}}(\text{B}) - \Delta G^0_{\text{solv}}(\text{A})], \tag{1}$$

where the gas-phase free energy is given by

$$\Delta G^0_g = \Delta E - RT \ln\left(\frac{Q^{\text{B}}}{Q^{\text{A}}}\right). \tag{2}$$

Here ΔE is the reaction energy; R is the Boltzmann constant; T is the temperature; Q^{A} and Q^{B} are the total partition functions evaluated with the zero of energy set at the bottom of each respective potential well.

This expression can be generalized for the free-energy profile of reaction in solution. In particular, the standard free energy at a point $\mathbf{R}(s)$ along the reaction coordinate s relative to that of the reactant A is expressed as

$$\Delta G^0_s(s) = \Delta G^0_s(\text{A} \rightarrow \mathbf{R}(s)) = V_{\text{MEP}}(s) - RT \ln\left(\frac{Q(\mathbf{R}(s))}{Q^{\text{A}}}\right) + \Delta G^0_{\text{solv}}(\mathbf{R}(s)) - \Delta G^0_{\text{solv}}(\text{A}), \tag{3}$$

where $V_{\text{MEP}}(s)$ is the gas-phase potential energy along the reaction coordinate s with the zero of energy set at the reactant. Equation (3) indicates that, *in order to obtain an accurate free energy profile for reaction in solution, one requires not only an accurate free energy of solvation but also an accurate gas-phase free-energy profile*. In calculations of free energies of activation of many reactions in solution, most previous studies have focused mostly on the solvation free-energy contributions and often overlooked errors in the calculated gas-phase free-energy profile.

The central issue here is how to define the reaction coordinate s. Adopting the reaction path Hamiltonian formalism, the reaction coordinate s for reactions in solution is defined as the distance along the minimum-free-energy path on the free-energy surface. However, following the reaction path on the solution-phase free-energy surface, as defined in equation (3), is almost an impossible task. The major difficulty arises from the necessity to perform normal mode analysis at every point on the gas-phase potential surface in order to calculate vibrational partition functions. To circumvent this problem, an assumption is made that the gas-phase Born–Oppenheimer potential energy surface $E(\mathbf{R})$ has similar topology to the gas-phase free-energy surface along the reaction coordinate. In this case, a pseudo-free-energy surface $G^*(\mathbf{R})$ in the solute nuclear coordinates $\mathbf{R}$ is related to $E(\mathbf{R})$ by the following expression:

$$G^*(\mathbf{R}) = E(\mathbf{R}) + \Delta G^0_{\text{solv}}(\mathbf{R}). \tag{4}$$

The pseudo-free-energy surface defined above allows one to utilize advanced computational methods that have been well developed for following reaction paths in the gas phase. Analogous to the gas phase, the reaction coordinate s in solution is defined as the distance along the MFEP which is the steepest-descent path from the transition state towards both the reactant(s) and the product(s) on the pseudo-free-energy surface $G^*(\mathbf{R})$. To obtain the free-energy profile of reaction in solution the gas-phase $-RT\ln(Q(s)/Q^A)$ term is added to the pseudo-free-energy profile $\Delta G^*(s)$. In summary, the procedure for calculating free-energy profiles of reaction in solution involves three steps.

(1) Select the appropriate level of theory and basis set that can give an accurate gas-phase free energy surface.
(2) Determine the transition state and calculate the MFEP on the solution pseudo-free-energy surface defined above.
(3) Add contributions from the gas-phase solute internal degrees of freedom along this MFEP. These contributions were mistakenly omitted in previous dielectric continuum calculations of free energies of activation including our own first study of solvent effects on the reaction profile of the S_N2 $Cl^- + CH_3Cl$ reaction [58].

Within the dielectric continuum solvation methodology, the free energy of solvation can be written as

$$\Delta G^0_{\text{solv}}(\mathbf{R}) = \Delta G_{\text{el}}(\mathbf{R}) + \Delta G_{\text{dis}}(\mathbf{R}) + \Delta G_{\text{rep}}(\mathbf{R}) + \Delta G_{\text{cav}}(\mathbf{R}), \tag{5}$$

where ΔG_{el} constitutes solvation terms of electrostatic nature, ΔG_{dis} and ΔG_{rep} are the solvent–solute dispersion and repulsion interactions respectively, and ΔG_{cav} is the work required to create the cavity. Note that contributions from the solute internal motions, such as shifts in the solute vibrational frequencies, are effectively included by fitting the cavity size to experimental free energies of hydration. There exist different methods for calculating each of these terms. Below I present one particular combination that was used in applications presented here and also has been working well in many of our studies.

5.2. *Generalized conductor-like screening model*

The GCOSMO model [38, 39, 52, 53, 58, 133, 134] is an *ab initio* generalization of the COSMO approach, which was first proposed by Klamt and Schüürmann and originally implemented at the semiempirical MO level [35]. This methodology is based on a fundamental classical electrostatic theory which states that the electrostatic potential on the boundary surface of a cavity in a conductor as well as inside the conductor is zero. Thus, the surface charges $\sigma(\mathbf{r})$ on the surface S of the cavity in a screening conductor (the dielectric constant $\varepsilon = \infty$) can be determined from such a boundary condition:

$$\sum_i \frac{z_i}{|\mathbf{r} - \mathbf{R}_i|} - \int_V \frac{\rho(\mathbf{r}')}{|\mathbf{r} - \mathbf{r}'|} \mathrm{d}^3 r' + \int_S \frac{\sigma(\mathbf{r}')}{|\mathbf{r} - \mathbf{r}'|} \mathrm{d}^2 r' = 0, \tag{6}$$

where $\mathbf{r}$ is on S, ρ is the solute electron density, and z_i and $\mathbf{R}_i$ are the nuclear charge and position vector of atom i. For a dielectric medium specified by the dielectric constant ε, the surface charges are then determined approximately by uniformly scaling the screening conductor surface charge σ by a factor of $f(\varepsilon) = (\varepsilon - 1)/\varepsilon$ to satisfy Gauss' theorem. Note that for water ($\varepsilon = 78.4$), this scaling factor is 0.987, that infers

water is behaving 99% like a perfect conductor. Thus, this approximation is not too unreasonable for polar solvents. In fact, in comparison with the exact Poisson's boundary condition used in the PCM, the average unsigned differences in hydration free energies between two models are less than 0.2 kcal mol^{-1} for neutral solutes and less than 0.9 kcal mol^{-1} for ions [133].

Within the boundary element approach, the cavity boundary is defined by M surface elements with areas $\{S_u\}$. The surface charge density at each surface element is approximated as a point charge $\{q_u\}$, located at the centre $\{\mathbf{t}_u\}$ of that element. From the above boundary condition, the total electrostatic solvation free energy is given by

$$\Delta G_{\text{els}}(\mathbf{q}) = \mathbf{z}\dagger\mathbf{B}\dagger\mathbf{q} + \mathbf{c}\dagger\mathbf{q} + \frac{1}{2f(\varepsilon)}\mathbf{q}\dagger\mathbf{A}\mathbf{q}, \tag{7}$$

where

$$\mathbf{q} = -f(\varepsilon)\mathbf{A}^{-1}(\mathbf{B}\mathbf{z} + \mathbf{c}), \tag{8}$$

is the vector of surface charges, **A**, **B** and **c** are $M \times M$, $M \times N$ and $M \times 1$ matrices respectively with matrix elements defined by

$$A_{uv} = \frac{1}{|\mathbf{t}_u - \mathbf{t}_v|} \text{ for } u \neq v, \text{ and } A_{uu} = 1.07\left(\frac{4\pi}{S_u}\right)^{1/2} \tag{9}$$

$$B_{ui} = \frac{1}{|\mathbf{t}_u - \mathbf{R}_i|'} \tag{10}$$

$$c_u = \sum_{\mu\nu} P_{\mu\nu} L^u_{\mu\nu'} \tag{11}$$

where

$$L^u_{\mu\nu} = -\left\langle \mu \left| \frac{1}{\mathbf{r} - \mathbf{t}_u} \right| \nu \right\rangle, \tag{12}$$

with $P_{\mu\nu}$ the density matrix element, and μ and ν basis functions. The dagger denotes matrix transposition. This electrostatic contribution to the free energy of solvation can be incorporated directly into the Fock matrix elements and can be solved simultaneously within a single self-consistent field (SCF) step for both the solute wavefunction and the surface charges. The pseudo-free energy of the whole system (solute + surface charges) is then given by

$$\begin{aligned} G^* = &\sum_{\mu\nu} P_{\mu\nu}[(H^0_{\mu\nu} + H^s_{\mu\nu}) + \tfrac{1}{2}(G^0_{\mu\nu} + G^s_{\mu\nu})] \\ &-\tfrac{1}{2}f(\varepsilon)\,\mathbf{z}\dagger\mathbf{B}\dagger\mathbf{A}^{-1}\mathbf{B}\mathbf{z} + E_{\text{nn}} + G_{\text{non-els}}, \end{aligned} \tag{13}$$

where E_{nn} is the solute nuclear repulsion and **z** is the vector of N nuclear charges. The solvent contributions to the one- and two-electron terms of the Fock matrix ($H_{\mu\nu}$ and $G_{\mu\nu}$ respectively) are expressed as

$$H^s_{\mu\nu} = -f(\varepsilon)\,\mathbf{z}\dagger\mathbf{B}\dagger\mathbf{A}^{-1}L_{\mu\nu}, \tag{14}$$

$$G^s_{\mu\nu} = -f(\varepsilon)\,\mathbf{c}\dagger\mathbf{A}^{-1}L_{\mu\nu}. \tag{15}$$

For the dispersion and short-range repulsion contributions, we adopted the method of Floris *et al.* [135]:

$$\Delta G_{\text{dis}} = \rho_{\text{H}_2\text{O}} \sum_i^N \sum_u^M \frac{2d_{i\text{H}} + d_{i\text{O}}}{3r^6_{iu}} (\mathbf{r}_{iu} \cdot \mathbf{n}_u)\, S_u, \tag{16}$$

$$\Delta G_{\text{rep}} = -\rho_{H_2O} \sum_{i}^{N} \sum_{u}^{M} \frac{2c_{iH} + c_{iO}}{9r_{iu}^{12}} (\mathbf{r}_{iu} \cdot \mathbf{n}_u) S_u, \tag{17}$$

where ρ_{H_2O} is the density number of water, d_{iH}, c_{iH} and d_{iO}, c_{iO} are dispersion and repulsion coefficients for interactions of the solute atom i with the solvent hydrogen and oxygen atoms respectively. These coefficients can be taken from available MM force fields, and we found that the OPLS force field [136] works well in most cases; $\mathbf{n}_u$ is the unit vector normal to the surface at the point $\mathbf{t}_u$ and directed inside the cavity; $\mathbf{r}_{iu}$ is the $(\mathbf{t}_u - \mathbf{R}_i)$ vector. The cavity size [137] in this case was increased to account for the solvent excluding region by adding 1.29 Å (our optimized radius of solvent water) to the solute atomic radii.

The cavity formation term is the work required to create the cavity in the solvent. Here we employed the scaled particle fluid theory of Pierotti [138], which was transformed by Huron and Claverie [139] into an atom–molecule-type formalism. In particular, ΔG_{cav} is given by

$$\Delta G_{\text{cav}} = \sum_{i=1}^{N} (K_0 + K_1 a_{is} + K_2 a_{is}^2 + K_3 a_{is}^3) \frac{S_i^{\text{exposed}}}{S_i}, \tag{18}$$

where K_i ($i = 0$–3) are functions of the temperature, pressure, density and hardsphere diameter of the solvent taken from the work of Huron and Claverie [139]. a_{is} is the atomic radius of atom i plus 1.4 Å, the radius of the water molecule. S_i^{exposed}/S_i is the fraction of the exposed surface of the solute atom i. These methods for calculating non-electrostatic contributions have been found to be sufficiently accurate from several previous studies [38, 135, 140–145].

5.2.1. *Analytical derivatives*

The pseudo-free energy given above in equation (13) can be rewritten as

$$G^* = \sum_{\mu\nu} P_{\mu\nu}(H_{\mu\nu}^0 + \tfrac{1}{2}G_{\mu\nu}^0) + E_{\text{nn}} + \Delta G_{\text{el}} + \Delta G_{\text{non-els}}, \tag{19}$$

where $H_{\mu\nu}^0$ and $G_{\mu\nu}^0$ are the solute one- and two-electron components respectively of the Fock matrix and involve only the solute electron–electron and electron–nuclei interactions, and ΔG_{el} and $\Delta G_{\text{non-els}}$ are the electrostatic and non-electrostatic components respectively of the solvation free energy. Applications of the free-energy. Applications of the free-energy derivatives so far have included only contributions from the electrostatic term. Without the non-electrostatic contributions, the derivative of the free energy in equation (19) with respect to the nuclear coordinates $\mathbf{R}_i$ of atom i is given by

$$\begin{aligned} \nabla_{\mathbf{R}_i}(G^*) = & \sum_{\mu\nu} P_{\mu\nu} \nabla_{\mathbf{R}_i}(H_{\mu\nu}^0) + \tfrac{1}{2} \sum_{\substack{\mu\nu \\ \lambda\sigma}} P_{\mu\nu} P_{\lambda\sigma} \nabla_{\mathbf{R}_i}(\mu\lambda \parallel \nu\sigma) \\ & + \nabla_{\mathbf{R}_i}(E_{\text{nn}}) - \sum_{\mu\nu} W_{\mu\nu} \nabla_{\mathbf{R}_i}(S_{\mu\nu}) \\ & + \mathbf{z}\dagger(\nabla_{\mathbf{R}_i}\mathbf{B}\dagger)\mathbf{q} + (\nabla_{\mathbf{R}_i}^*\mathbf{c}\dagger)\mathbf{q} + \frac{1}{2f}\mathbf{q}\dagger(\nabla_{\mathbf{R}_i}\mathbf{A})\mathbf{q}. \end{aligned} \tag{20}$$

The first four terms have the same expressions as the Hartree–Fock (HF) or Kohn–Sham DFT theory for a gas-phase molecule except that the density matrix $P_{\mu\nu}$ and the energy-weighted density matrix $W_{\mu\nu}$ contain the solvent effects. The last

three terms are due to the electrostatic solvation energy. They are from the interactions of surface charges with solute nuclear charges, with solute electron charge distribution and with other surface charges respectively. Note that, with the conductor-like screening boundary condition, terms involving the derivative of the surface charges are not needed. If the atomic radii used to define the cavity are assumed to be fixed, and surface elements stick to the atom to which they belong, then from [35]

$$\nabla_{\mathbf{R}_i}(A_{uv}) = -\frac{\mathbf{t}_u - \mathbf{t}_v}{|\mathbf{t}_u - \mathbf{t}_v|^3}\nabla_{\mathbf{R}_i}(\mathbf{t}_u - \mathbf{t}_v) = -\frac{\mathbf{t}_u - \mathbf{t}_v}{|\mathbf{t}_u - \mathbf{t}_v|^3}(\theta_{ui} - \theta_{vi}), \tag{21}$$

with

$$\theta_{ui} = \begin{cases} 0 & \text{for } u \notin \text{sphere of atom } i, \\ 1 & \text{for } u \in \text{sphere of atom } i. \end{cases} \tag{22}$$

The derivative $\nabla_{\mathbf{R}_i}(\mathbf{A}_{uu})$ of the diagonal elements of $\mathbf{A}$ depends on $\partial S_u/\partial \mathbf{R}_i$, that is the change in the surface area of the element u with respect to the change in the position of atom i. Thus, only surface elements at the overlapping regions of the atomic sphere of atom i with the neighbour spheres have non-zero $\partial S_u/\partial \mathbf{R}_i$. Numerical analysis indicated that it is reasonable to assume that

$$\nabla_{\mathbf{R}_i}(A_{uu}) = 0. \tag{23}$$

Finally, differentiating B_{uj} and c_u in equations (10) and (11), we obtain

$$\nabla_{\mathbf{R}_i}(B_{uj}) = -\frac{\mathbf{t}_u - \mathbf{R}_j}{|\mathbf{t}_u - \mathbf{R}_j|^3}\nabla_{\mathbf{R}_i}(\mathbf{t}_u - \mathbf{R}_j) = -\frac{(\mathbf{t}_u - \mathbf{R}_j)}{|\mathbf{t}_u - \mathbf{R}_j|^3}(\theta_{ui} - \delta_{ij}), \tag{24}$$

$$\nabla^*_{\mathbf{R}_i}(c_u) = \sum_{\mu\nu} P_{\mu\nu}\left\langle \mu \left| \frac{\mathbf{r} - \mathbf{t}_u}{|\mathbf{r} - \mathbf{t}_u|^3}(-\nabla_{\mathbf{R}_i}(\mathbf{t}_u)) \right| \nu \right\rangle = -\sum_{\mu\nu} P_{\mu\nu}\left\langle \mu \left| \frac{(\mathbf{r} - \mathbf{t}_u)}{|\mathbf{r} - \mathbf{t}_u|^3}\theta_{ui} \right| \nu \right\rangle. \tag{25}$$

The asterisk denotes that equation (25) is not the complete derivative $\nabla_{\mathbf{R}_i}(c_u)$; the term containing the partial derivative of the density matrix, $P_{\mu\nu}$ has already been included in the fourth term of equation (20).

The second derivative of the pseudo-free energy with respect to the $\mathbf{R}_i$ and $\mathbf{R}_j$ solute nuclear coordinates can be obtained by differentiating the first derivative given in equation (20). The explicit expression has been published elsewhere [39].

The simplicity of the expressions for the contributions of solvent polarization to the Fock matrix and its derivatives gives the GCOSMO model many computational advantages. The most significant is that the computational cost for calculations of energy, gradient and Hessian is no more than 15% larger than that of the corresponding gas-phase calculations. Furthermore, in many cases, the external polarization field localizes the wavefunction and hence reduces the number of SCF iterations.

5.2.2. *Other aspects of the model*

5.2.2.1. *Outlying charge effect.* This effect arises from the fact that implementation of any *classical* continuum solvation model within a QM level will cause a small portion of the electronic density distribution to be outside the cavity regardless of the cavity size. Recent studies [146, 147] have proposed several post-SCF correction schemes to account for this effect. In my view, such schemes philosophically attempt to make the dielectric continuum methodology more rigorous than it should be. Comments below regarding cavity size further support this view. In addition, these schemes add a layer of complication when one requires the inclusion of the outlying charge effect in free-energy derivatives for consistency in the determination of the structure and reaction

path; yet the atomic radii used in specifying the cavity size are still needed to be optimised to account for other effects. For these reasons, outlying charge effects were not considered in the GCOSMO model. One positive aspect, however, is that the proposed schemes remove most of the rather strong basis set dependence on solvation free energies of anions where the solute wavefunctions are rather diffuse.

5.2.2.2. *Cavity specification.* This is perhaps the most controversial aspect of the use of the dielectric continuum approach. There is no rigorous way to define the cavity boundary. However, it is generally accepted that the molecule-shaped cavity provides a more realistic description than a simple spherical or ellipsoidal cavity. The size of such a cavity is specified by the atomic radii. These atomic radii have similar magnitudes to van der Waals atomic radii used in MM force fields, although most have been optimized for a particular solvation model. Furthermore, there are three different ways to define the boundary surface, namely van der Waals (overlapping spheres), solvent-accessible [137] or solvent-excluding [148] surface. For reactions in solution, we found that the solvent-excluding surface provides more stable results owing to its smooth nature. In all applications presented below, the solvent-excluding surface was used. It was constructed using the GEPOL algorithm [149]. The atomic radii (N, 1.74 Å; C, 2.10 Å; H, 1.17 Å; Cl, 1.75 Å) used have been optimized at the HF/6-31G(d) level using the GCOSMO model to reproduce free energies of hydration for a representative set of small molecules and ions [133]. By optimizing the atomic radii for determining the cavity, other contributions that were not explicitly considered in the model are effectively included.

5.3. *Illustrative examples*

5.3.1. *S_N2 $Cl^- + CH_3Cl$ charge-transfer reaction*

The first example is the $Cl^- + CH_3Cl$ biomolecular nucleophilic substitution (S_N2) reaction in the gas phase and aqueous solution. To calculate the free-energy profile of this reaction in aqueous solution, first one needs to determine the level of theory required for accurate calculations of the gas-phase potential curve. By comparison with the accurate *ab initio* MO calculations and available experimental data, the hybrid density functional theory, particularly the Becke half-and-half exchange and Lee–Yang–Parr correlation (BH & HLYP) functional method was found to give the best overall performance among existing DFT methods and can predict accurate structural, energy and vibrational frequency information not only for equilibrium structures but also for the transition state with quality comparable with the second-order Møller–Plesset (MP2) level of theory [58]. In particular, the calculated classical barrier of 2.6 kcal mol^{-1} compared favourably with the semiempirical value of 3.1 kcal mol^{-1} that was fitted to the experimental thermal rate constant at the room temperature. Similarly, the complex binding energy was slightly overestimated to be -9.9 kcal mol^{-1} compared with the experimental data of -8.6 ± 0.2 kcal mol^{-1}. In the second step, one can in principle optimize the transition state in solution and then determine the MFEP by following the steepest-descent path from the transition state. However, most previous simulations have used a much simpler reaction coordinate R_C defined by Chandrasekhar *et al.* [111] as

$$R_C = R_{CCl'} - R_{CCl},$$

where Cl′ is the leaving atom. To facilitate comparisons with results from previous simulations, the same reaction coordinate was used. As shown in figure 1, the

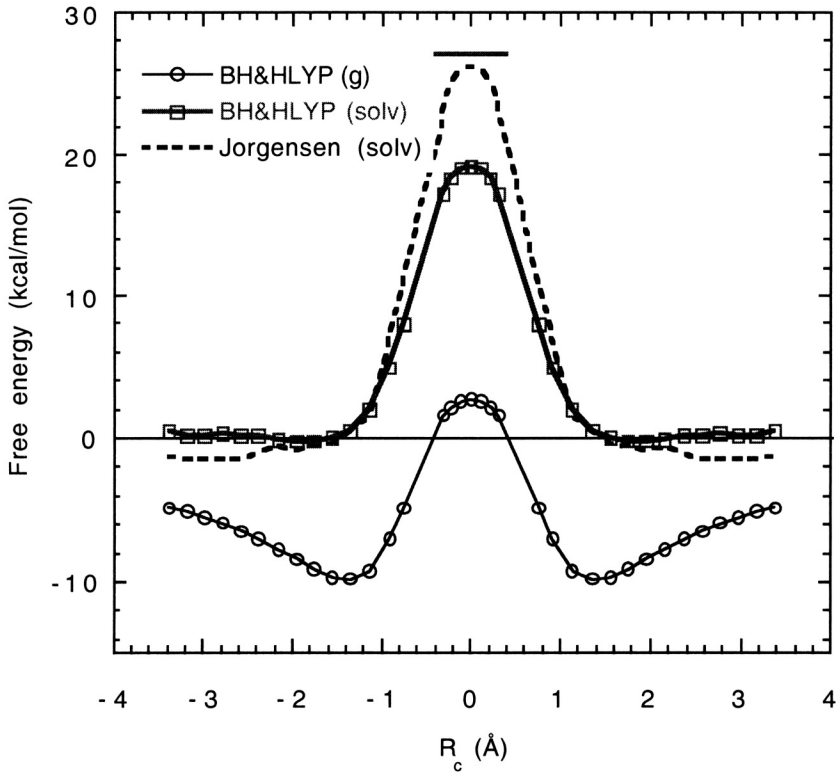

Figure 1. Reaction profiles of the S_N2 $Cl^- + CH_3Cl'$ reaction in the gas phase (potential energy) (thin solid curve) and in aqueous solution (pseudo-free energy) (thick solid curve). The solid curves are from the BH & HLYP–GCOSMO calculations using the 6-31 + G(d, p) basis set, and the broken curve is from MC simulations [111]. The horizontal bar is the free energy of activation with added contribution from the solute internal degrees of freedom.

unimodal shape of the free-energy curve calculated from the methodology described above agrees well with that obtained from classical MC simulations. In particular, the calculated free energy of activation of 27.5 kcal mol^{-1} is in good accord with the previous MC result of 26.3 ± 0.5 kcal mol^{-1} [111], the MD result of 27.7 kcal mol^{-1} [112] and the experimental value of 26.6 kcal mol^{-1}. Figure 2 shows individual contributions, namely electrostatic, dispersion, repulsion and cavitation, to the hydration free energy along the reaction coordinate. The results confirm that the non-electrostatic contribution has only a small effect on the free energy of activation [112]. In particular, the overall non-electrostatic contribution, resulting mostly from the cavity formation term (see figure 2), is found to lower the barrier by about 2 kcal mol^{-1} while the electrostatic contribution effectively raises the barrier by 19 kcal mol^{-1}.

5.3.2. *The Menshutkin* $NH_3 + CH_3CL \rightarrow H_3NCH_3^+ + Cl^-$ *reaction*

First of all, to determine an appropriate level of theory for accurate potential and free energy surfaces, benchmark gas-phase single point fourth-order Moller–Plesser MP4(SDTQ) calculations at the MP2 optimized geometries at the stationary points using a large aug-cc-pVDZ [150] basis set were performed. Comparing with this benchmark result of 32.1 kcal mol^{-1} for the classical reaction barrier $\Delta V\ddagger$, MP2/6-31G(d, p) calculations overestimate by 6.3 kcal mol^{-1} while the BH & HLYP method

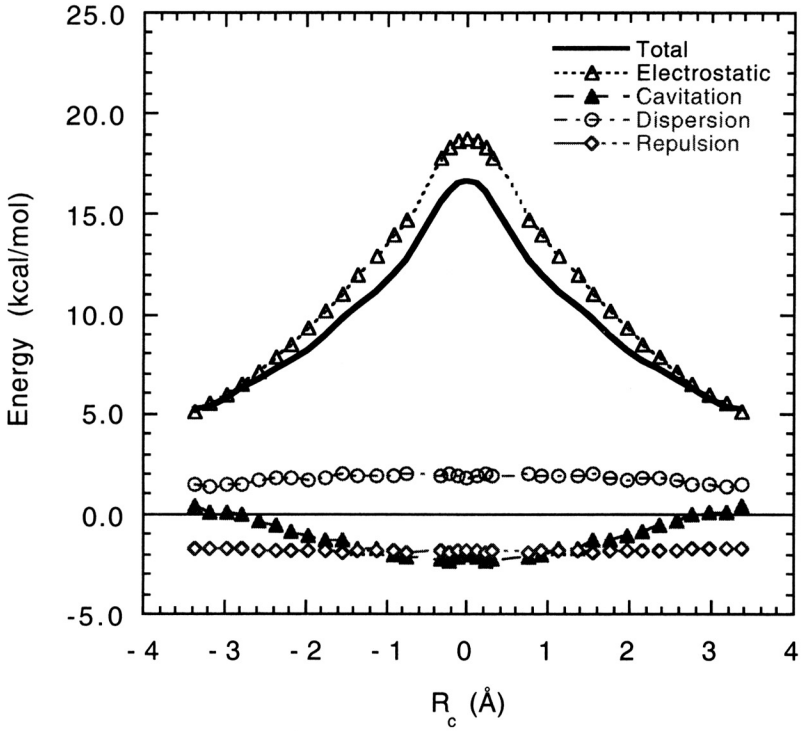

Figure 2. BH & HLYP/6-31 + G(d, p) total hydration energy (——) and its individual contributions ((△), electrostatic; (▲), cavitation; (○), dispersion; (◇), repulsion) plotted as functions of the reaction coordinate R_C of the S_N2 $Cl^- + CH_3Cl'$ reaction. All contributions are relative to their separated reactant values.

with the same basis set agrees to within 0.5 kcal mol^{-1}. When comparing the structural, energy and frequency information, overall the BH & HLYP results are closer to both MP4 and experiment than are the MP2 result [53]. This is consistent with conclusions from other studies [5, 151–153] that the BH & HLYP DFT method was found to be a computationally efficient and sufficiently accurate method for calculating transition-state properties.

Using the GCOSMO dielectric continuum methodology, the transition state of the Menshutkin $NH_3 + CH_3Cl \leftrightarrow NH_3CH_3^+ + Cl^-$ reaction in an aqueous solution was fully optimized and the MFEP in all degrees of freedom of the solute was determined by following the steepest-descent path on the pseudo-free-energy surface defined above and then corrected by adding the contribution from the gas-phase solute internal degrees of freedom.

In figure 3 we plot the CN and CCl bond distances and the HCN angle along both the gas-phase MEP and solution-phase MFEP. These internal coordinates show the largest changes as functions of the reaction coordinate. For the reaction in water, they are shifted in the product direction. This means that solvent effects advance the reaction coordinate. In particular, at the transition state as shown in figure 4, solvent effects elongate the CN bond by 0.42 Å, shorten the CCl bond by 0.30 Å and reduce the HCN angle by 14°. These shifts are somewhat larger than those obtained from the reaction field factor method at the HF level [49]. Since electron correlation was found to be important for the gas-phase transition-state geometry (it shortens the CN bond by 0.1 Å), one expects the solvent effects on the structure also to be very different for

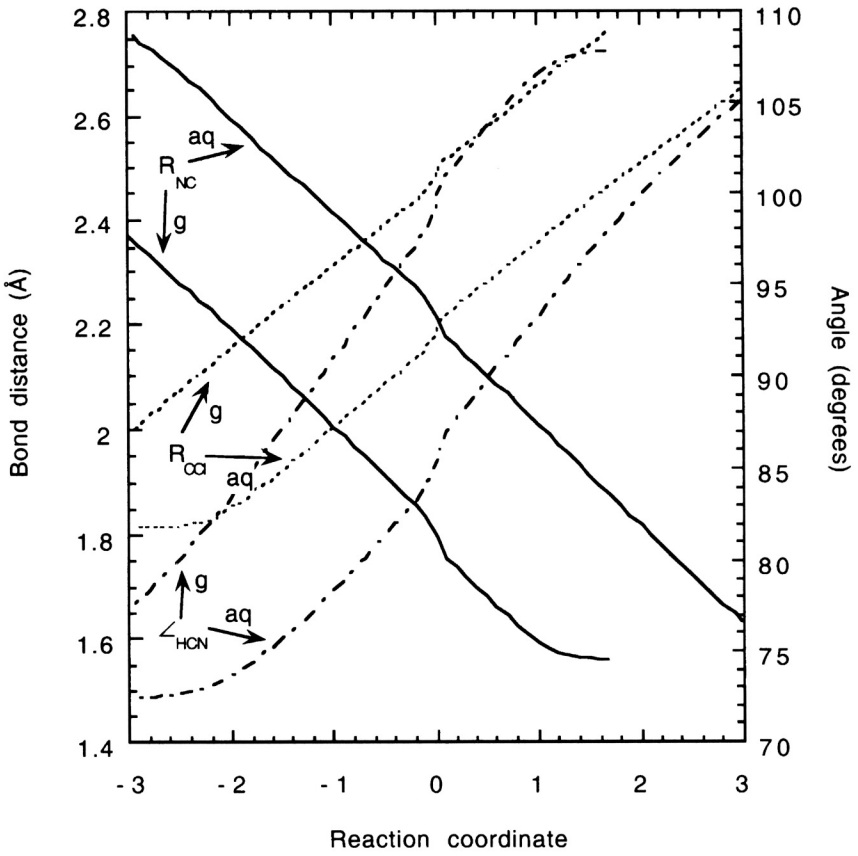

Figure 3. Bond distances NC and CCl and angle HCN as functions of the reaction coordinates for the Menshutkin $NH_3 + CH_3Cl$ reaction in both the gas phase (g) and aqueous solution (aq). The origin of the reaction coordinate is at the saddle point in each case.

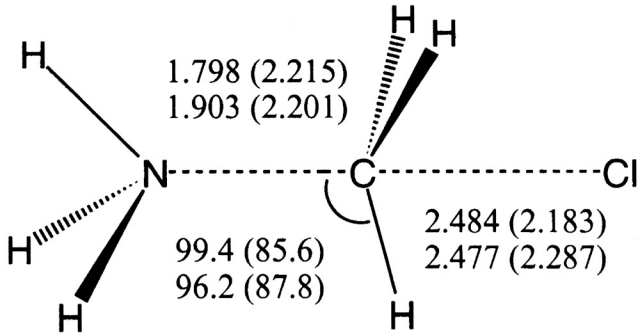

Figure 4. Optimized geometries of the transition state of the Menshutkin $NH_3 + CH_3Cl$ reaction in the gas phase and in aqueous solution (in parentheses). The distances are in ångströms and the angle is in degrees. Values in the second rows were calculated at the HF/6-31-G** level using the reaction field factor method (taken from [48]).

the HF and DFT results. The large shift in the transition state can be understood from the fact that the Menshutkin reaction is a charge separation process. Aqueous solvent facilitates charge separation by gaining a favourable free energy of solvation. These

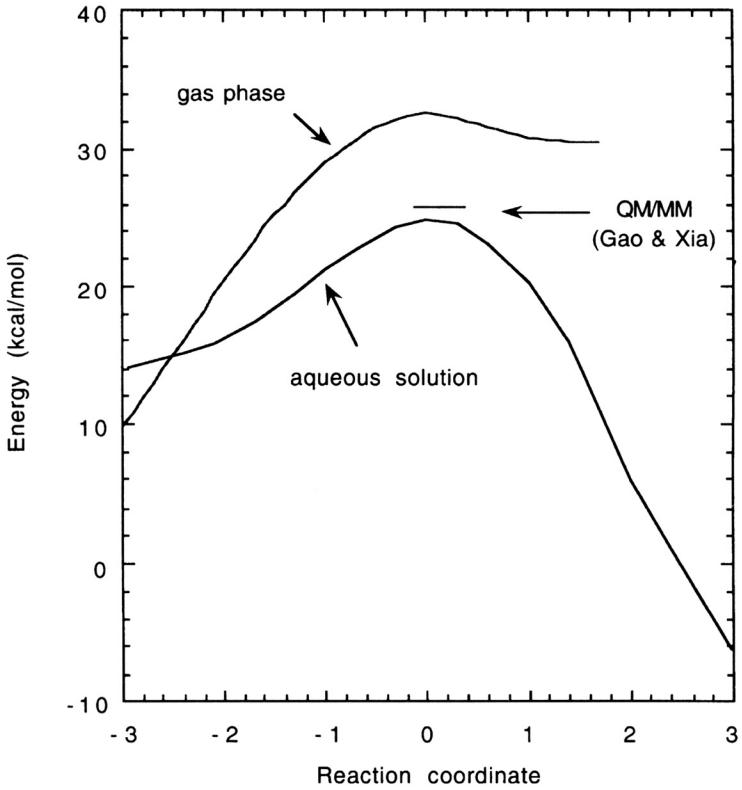

Figure 5. Free-energy profiles along the gas-phase MEP and solution-phase MFEP of the Menshutkin NH_3+CH_3Cl reaction. The QM–MM free energy of activation is taken from [117].

trends are consistent with previous results from the PCM [119] and semiempirical AM1–MM MC simulations [117].

Free-energy profiles in both the gas phase and aqueous solution are also plotted in figure 5. For formation of the gas-phase ion products $H_3CNH_3^+$ and Cl^-, the reaction is 110 kcal mol^{-1} endothermic. Thus, the dynamical bottleneck is located far in the exit channel. Solvent effects change the reaction energetics to noticeably exothermic, thus shifting this bottleneck significantly towards the entrance channel and decreasing the free energy of activation to 24.8 kcal mol^{-1}. This free energy of activation agrees well with the value of 26.3 kcal mol^{-1} from the AM1–MM MC simulations of Gao and Xia, the reaction field factor result of 28.7 kcal mol^{-1} [49] and the experimental value of 23.5 kcal mol^{-1} [154] for a similar Menshutkin reaction NH_3+CH_3I in water.

6. Conclusion and future outlook

The simplicity of the dielectric continuum solvation approach provides many computational advantages for quantum modelling of reactions in solution. The availability of free-energy derivatives in models based on a molecule-shaped cavity greatly enhances the ability of these models to explore free-energy surfaces, to optimize and to characterize transition states. The additional computational cost is only a fraction of the corresponding gas-phase calculation and is much smaller than those of MC or MD simulations. For these reasons, condensed-phase quantum chemistry studies using dielectric continuum methodology are becoming more routine.

Despite these positive aspects, work remains to be done. In particular, more attention should be given to the hydrophobic effects on the free energy of activation and the transition-state structure of reaction in solution. For many reactions, such effects are not negligible even in polar solvents. In addition, work has already begun to extend the dielectric continuum methodology to include non-equilibrium solvation effects for addressing dynamics of reactions in solution.

Acknowledgments

I am grateful to Dr Eugene V. Stefanovich, Thanh-Thai T. Truong and Uyen Nguyen for their contributions to this work. This work is supported in part by the National Science Foundation via a Young Investigator Award.

References

[1] Cramer, C. J., and Truhlar, D. G., 1994, *Reviews in Computational Chemistry*, edited by K. B. Lipkowitz and D. B. Boyd (New York: VCH), p. 1.
[2] Tomasi, J., and Persico, M., 1994, *Chem. Rev.*, **94**, 2027.
[3] Cramer, C. J., and Truhlar, D. G., 1996, *Solvent Effects and Chemical Reactivity*, edited by O. Tapia and J. Bertrán (Dordrecht: Kluwer), p. 1.
[4] Pullman, A., and Pullman, B., 1975, *Q. Rev. Biophys.*, **7**, 505.
[5] Zhang, Q., Bell, R., and Truong, T. N., 1995, *J. phys. Chem.*, **99**, 592.
[6] Siegbahn, P. E. M., 1996, *J. phys. Chem.*, **100**, 14672.
[7] Hirao, K., and Kebarle, P., 1989, *Can. J. Chem.*, **67**, 1262.
[8] Morokuma, K., 1982, *J. Am. chem. Soc.*, **104**, 3732.
[9] Jensen, J. H., and Gordon, M. S., 1995, *J. Am. chem. Soc.*, **117**, 8159.
[10] Chipot, C., Gorb, L. G., and Rivail, J. L., 1994, *J. phys. Chem.*, **98**, 1601.
[11] Car, R., and Parrinello, M., 1985, *Phys. Rev. Lett.*, **55**, 2471.
[12] Laasonen, K., Sprik, M., Parrinello, M., and Car, R., 1993, *J. chem. Phys.*, **99**, 9080.
[13] Fois, E. S., Sprik, M., and Parrinello, M., 1994, *Chem. Phys. Lett.*, **223**, 411.
[14] Jorgensen, W. L., 1989, *Accts Chem. Res.*, **22**, 184.
[15] Aqvist, J., and Warshel, A., 1993, *Chem. Rev.*, **93**, 2523.
[16] Gao, J., 1996, *Reviews in Computational Chemistry*, edited by K. B. Lipkowitz and D. B. Boyd (New York: VCH), p. 119.
[17] Singh, U. C., and Kollman, P. A., 1986, *J. comput. Chem.*, **7**, 718.
[18] Field, M. J., 1993, *Computer Simulation of Biomolecular Systems: Theoretical and Experimental Applications*, edited by W. F. van Gunsteren, P. K. Weiner and A. J. Wilkinson (Leiden: ESCOM), p. 82.
[19] Field, J. J., Bash, P. A., and Karplus, M., 1990, *J. comput. Chem.*, **11**, 700.
[20] Day, P. N., Jensen, J. H., Gordon, M. S., Webb, S. P., Stevens, W. J., Krauss, M., Garmer, D., Basch, H., and Cohen, D., 1996, *J. chem. Phys.*, **105**, 1968.
[21] Stefanovich, E. V., and Truong, T. N., 1996, *J. chem. Phys.*, **104**, 2946.
[22] Wesolowski, T. A., and Warshel, A., 1993, *J. phys. Chem.*, **97**, 8050.
[23] Hirata, F., and Rossky, P. J., 1981, *Chem. Phys. Lett.*, **83**, 329.
[24] Hirata, F., Rossky, P. J., and Pettitt, B. M., 1983, *J. chem. Phys.*, **78**, 4133.
[25] Luzhkov, V., and Warshel, A., 1992, *J. comput. Chem.*, **13**, 199.
[26] Miertus, S., Scrocco, E., and Tomasi, J., 1981, *Chem. Phys.*, **55**, 117.
[27] Cammi, R., and Tomasi, J., 1994, *J. chem. Phys.*, **100**, 7495.
[28] Cammi, R., and Tomasi, J., 1994, *J. chem. Phys.*, **101**, 3888.
[29] Cossi, M., Tomasi, J., and Cammi, R., 1995, *Int. J. quant. Chem.*, *S***29**, 695.
[30] Dillet, V., Rinaldi, D., Angyan, J. G., and Rivail, J. L., 1993, *Chem. Phys. Lett.*, **202**, 18.
[31] Dillet, V., Rinaldi, D., and Rivail, J. L., 1994, *J. phys. Chem.*, **98**, 5034.
[32] Kirkwood, J. G., 1934, *J. chem. Phys.*, **2**, 351.
[33] Tannor, D. J., Marten, B., Murphy, R., Friesner, R. A., Sitkoff, D., Nicholls, A., Ringnalda, M., Goddard, W. A., and Honig, B., 1994, *J. Am. chem. Soc.*, **116**, 11875.

[34] Cortis, C. M., Langlois, J.-M., Beachy, M. D., and Friesner, R. A., 1996, *J. chem. Phys.*, **105**, 5472.
[35] Klamt, A., and Schüürmann, G., 1993, *J. chem. Soc., Perkin Trans. II*, 799.
[36] Andzelm, J., Kölmel, C., and Klamt, A., 1995, *J. chem. Phys.*, **103**, 9312.
[37] Baldridge, K., and Klamt, A., 1997, *J. chem. Phys.*, **106**, 6622.
[38] Truong, T. N., and Stefanovich, E. V., 1995, *Chem. Phys. Lett.*, **240**, 253.
[39] Truong, T. N., and Stefanovich, E. V., 1995, *J. chem. Phys.*, **103**, 3709.
[40] Huston, S. E., Rossky, P. J., and Zichi, D. A., 1989, *J. Am. chem. Soc.*, **111**, 5680.
[41] Lim, D., and Jorgensen, W. L., 1996, *J. phys. Chem.*, **100**, 17490.
[42] Ruiz-López, M. F., Rinaldi, D., and Bertran, J., 1995, *J. chem. Phys.*, **103**, 9249.
[43] Gao, J., and Xia, X., 1993, *J. Am. chem. Soc.*, **115**, 9667.
[44] Basilevsky, M. V., Chudinov, G. E., and Napolov, D. V., 1993, *J. phys. Chem.*, **97**, 3270.
[45] Gao, J., 1991, *J. Am. chem. Soc.*, **113**, 7796.
[46] Alemán, C., Maseras, F., Lledos, A., Duran, M., and Bertrán, J., 1989, *J. phys. org. Chem.*, **2**, 611.
[47] Takahashi, O., Sawahata, H., Ogawa, Y., and Kikuchi, O., 1997, *J. molec. Struct. (Theochem.)*, **393**, 141.
[48] Kikuchi, O., Sano, Y., Takahashi, O., and Morihashi, K., 1996, *Heteroat. Chem.*, **7**, 273.
[49] Dillet, V., Rinaldi, D., Bertrán, J., and Rivail, J., 1996, *J. chem. Phys.*, **104**, 9437.
[50] Aguilar, M., Bianco, R., Miertus, S., Persico, M., and Tomasi, J., 1993, *Chem. Phys.*, **174**, 397.
[51] Sato, H., and Kato, S., 1994, *J. molec. Struct. (Theochem.)*, **116**, 67.
[52] Truong, T. N., and Stefanovich, E. V., 1995, *J. phys. Chem.*, **99**, 14700.
[53] Truong, T. N., Truong, T.-T. T., and Stefanovich, E. V., 1997, *J. chem. Phys.*, **107**, 1881.
[54] Hodoscek, M., and Hadzi, D., 1989, *J. molec. Struct.*, **198**, 461.
[55] Kurz, J. L., 1989, *J. Am. chem. Soc.*, **111**, 8631.
[56] Tortonda, F. R., Pascual-Ahuir, J.-L., Silla, E., and Tuñón, I., 1993, *J. phys. Chem.*, **97**, 11087.
[57] Tortonda, F. R., Pascual-Ahuir, J.-L., Silla, E., and Tuñón, I., 1995, *J. phys. Chem.*, **99**, 12525.
[58] Truong, T. N., Nguyen, U. N., and Stefanovich, E. V., 1996, *Int. J. quant. Chem.*, **60**, 1615.
[59] Assfeld, X., Sordo, J. A., Gonzalez, J., Ruizlopez, M. F., and Sordo, T. L., 1993, *J. molec. Struct. (Theochem)*, **106**, 193.
[60] Assfeld, X., Ruiz-López, M. F., Gonzalez, J., López, R., Sordo, J. A., and Sordo, T. L., 1994, *J. comput. Chem.*, **15**, 479.
[61] Bernardi, F., Pappalardo, R. R., Robb, M. A., and Venturini, A., 1995, *J. molec. Struct. (Theochem.)*, **357**, 33.
[62] Cossio, F. P., Roa, G., Lecea, B., and Ugalde, J. M., 1995, *J. Am. chem. Soc.*, **117**, 12306.
[63] Domingo, L. R., Picher, M. T., Andres, J., Moliner, V., and Safont, V. S., 1996, *Tetrahedron*, **52**, 10693.
[64] Essefar, M., El Mouhtadi, M., Liotard, D., and Abboud, J.-L. M., 1988, *J. chem. Soc., Perkin Trans. II*, 143.
[65] Fang, D., and Fu, X., 1996, *Chem. Phys. Lett.*, **259**, 265.
[66] Karcher, T., Sicking, W., Sauer, J., and Sustmann, R., 1992, *Tetrahedron Lett.*, **33**, 8027.
[67] Lecea, B., Arrieta, A., Roa, G., Ugalde, J. M., and Cossio, F. P., 1994, *J. Am. chem. Soc.*, **116**, 9613.
[68] Lecea, B., Arrieta, A., Lopez, X., Ugalde, J. M., and Cossio, F. P., 1995, *J. Am. chem. Soc.*, **117**, 12314.
[69] Lecea, B., Arrastia, I., Arrieta, A., Roa, G., Lopez, X., Arriortua, M. I., Ugalde, J. M., and Cossio, F. P., 1996, *J. org. Chem.*, **61**, 3070.
[70] Lopez, R., Suarez, D., Ruiz-Lopez, M. F., Gonzalez, J., Sordo, J. A., and Sordo, T. L., 1995, *J. chem. Soc., chem. Commun.*, **16**, 1677.
[71] Rastelli, A., Bagatti, M., and Gandolfi, R., 1995, *J. Am. chem. Soc.*, **117**, 4965.
[72] Reguero, M., Pappalardo, R. R., Robb, M. A., and Rezpa, H. S., 1993, *J. chem. Soc., Perkin Trans. II*, **8**, 1499.

[73] SPERLING, D., MEHLHORM, A., REISSIG, H. U., and FABIAN, J., 1996, *Liebigs' Ann.*, 1615.
[74] SUSTMANN, R., and SICKING, W., 1992, *Tetrahedron*, **48**, 10293.
[75] ANDRES, J., BOHM, S., MOLINER, V., SILLA, E., and TUNON, I., 1994, *J. phys. Chem.*, **98**, 6955.
[76] PARDO, L., OSMAN, R., WEINSTEIN, H., and RABINOWITZ, J. R., 1993, *J. Am. chem. Soc.*, **115**, 8263.
[77] CIEPLAK, A. S., and WIBERG, K. B., 1992, *J. Am. chem. Soc.*, **114**, 9226.
[78] ASSFELD, X., GARAPON, J., RINALDI, D., RUIZ-LOPEZ, M. F., and RIVAIL, J. L., 1996, *J. molec. Struct. (Theochem.)*, **371**, 107.
[79] YU, H.-A., and KARPLUS, M., 1990, *J. Am. chem. Soc.*, **112**, 5706.
[80] ANDRÉS, J., BOHM, S., MOLINER, V., SILLA, E., and TUÑÓN, I., 1994, *J. phys. Chem.*, **98**, 6955.
[81] ASSFELD, X., RUIZ-LOPEZ, M. F., GARCIA, J. I., MAYORAL, J. A., and SALVATELLA, L., 1995, *J. chem. Soc., chem. Commun.*, **13**, 1371.
[82] CATIVIELA, C., GARCIA, J. I., MAYORAL, J. A., ROYE, A. J., SALVATELLA, ASSFELD, I. X., and RUIZ-LOPEZ, M. F., 1992, *J. phys. org. Chem.*, **5**, 230.
[83] CATIVIELA, C., DILLET, V., GARCÍA, J. I., MAYORAL, J. A., RUIZ-LÓPEZ, M. F., and SALVATELLA, L., 1995, *J. molec. Struct. (Theochem.)*, **331**, 37.
[84] DE PASCUAL-TERESA, B., GONZALEZ, J., ASENSIO, A., and HOUK, K. N., 1995, *J. Am. chem. Soc.*, **117**, 4347.
[85] MCCARRICK, M. A., WU, Y. D., and HOUK, K. N., 1993, *J. org. Chem.*, **58**, 3330.
[86] RUIZ-LÓPEZ, M. F., ASSFELD, X., GARCÍA, J. I., MAYORAL, J. A., and SALVATELLA, L., 1993, *J. Am. chem. Soc.*, **15**, 8780.
[87] SALZNER, U., BACHRACH, S. M., and MULHEARN, D. C., 1997, *J. comput. Chem.*, **18**, 198.
[88] SUÁREZ, D., ASSFELD, X., GONZÁLEZ, J., RUIZ-LÓPEZ, M. F., SORDO, T. L., and SORDO, J. A., 1994, *J. chem. Soc., chem. Commun.*, 1683.
[89] NGUYEN, M. T., RASPOET, G., and VANQUICKENBORNE, L. G., 1997, *J. Am. chem. Soc.*, **119**, 2552.
[90] MOLINER, V., CASTILLO, R., SAFRONT, V. S., OLIVA, M., BOHN, S., TUNON, I., and ANDRES, J., 1997, *J. Am. chem. Soc.*, **119**, 1941.
[91] JONES-HERTZOG, D. K., and JORGENSEN, W. L., 1995, *J. Am. chem. Soc.*, **117**, 9077.
[92] JEMMIS, E. D., GIJU, K. T., and LESZCZYNSKI, J., 1997, *J. phys. Chem.* A, **101**, 7389.
[93] HALL, R. J., DAVIDSON, M. M., BURTON, N. A., and HILLIER, I. H., 1995, *J. phys. Chem.*, **99**, 921.
[94] DAVIDSON, M. M., HILLIER, I. H., and VINCENT, M. A., 1995, *Chem. Phys. Lett.*, **246**, 536.
[95] DAVIDSON, M. M., HILLIER, I. H., HALL, R. J., and BURTON, N. A., 1994, *J. Am. chem. Soc.*, **116**, 9294.
[96] ARNAUD, R., DILLET, V., PELLOUX-LEON, N., and VALLE, Y., 1996, *J. chem. Soc., Perkin Trans. II*, 2065.
[97] ADAMO, C., and LELJ, F., 1995, *Int. J. quant. Chem.* **56**, 645.
[98] ANDRES, J. L., LLEDOS, A., and BERTRAN, J., 1994, *Chem. Phys. Lett.*, **223**, 23.
[99] WONG, M. W., LEUNG-TOUNG, R., and WENTRUP, C., 1993, *J. Am. chem. Soc.*, **115**, 2465.
[100] LEE, D., KIM, C. K., LEE, B., LEE, I., and LEE, B. C., 1997, *J. comput. Chem.*, **18**, 56.
[101] RAUHUT, G., 1996, *J. comput. Chem.*, **17**, 1848.
[102] BARONE, V., and ADAMO, C., 1995, *J. phys. Chem.*, **99**, 15062.
[103] RIVAIL, J. L., and RINALDI, D., 1976, *Chem. Phys.*, **18**, 233.
[104] INGOLD, C. K., 1969, *Structure and Mechanism in Organic Chemistry*, second edition (Ithaca, New York: Cornell University Press).
[105] HYNES, J. T., 1985, *Theory of Chemical Reaction Dynamics*, edited by M. Baer (Boca Raton, Florida: CRC Press), p. 171.
[106] KREEVOY, M. M., and TRUHLAR, D. G., 1986, *Investigation of Rates and Mechanisms of Reactions*, edited by C. F. Bernasconi (New York: Wiley), p. 13.
[107] SHAIK, S. S., SCHLEGEL, H. B., and WOLFE, S., 1992, *Theoretical Aspects of Physical Organic Chemistry, The S_N2 Mechanisms* (New York: Wiley).
[108] MINKIN, V. I., SIMKIN, B. Y., and MINYAEV, R. M., 1990, *Quantum Chemistry of Organic Compounds—Mechanisms of Reactions* (Berlin: Springer).
[109] OLMSTEAD, W. N., and BRAUMAN, J. I., 1977, *J. Am. chem. Soc.*, **99**, 4219.
[110] ALBERY, W. J., 1980, *A. Rev. phys. Chem.*, **31**, 227.

[111] CHANDRASEKHAR, J., SMITH, S. F., and JORGENSEN, W. L., 1985, *J. Am. chem. Soc.*, **107**, 154.
[112] BASH, P. A., FIELD, M. J., and KARPLUS, M., 1987, *J. Am. chem. Soc.*, **109**, 8092.
[113] SINGH, U. C., and KOLLMAN, P. A., 1986, *J. comput. Chem.*, **7**, 718.
[114] MATHIS, J. R., BIANCO, R., and HYNES, J. T., 1994, *J. molec. Liquids*, **61**, 81.
[115] HWANG, J.-K., KING, G., CREIGHTON, S., and WARSHEL, A., 1988, *J. Am. chem. Soc.*, **110**, 5297.
[116] OHTA, K., and MOROKUMA, K., 1985, *J. phys. Chem.*, **89**, 5845.
[117] GAO, J., and XIA, X., 1993, *J. Am. chem. Soc.*, **115**, 9667.
[118] ISSACS, N. S., 1987, *Physical Organic Chemistry* (New York: Wiley).
[119] SOLÀ, M., LLEDÓS, A., DURAN, M., BERTRÁN, J., and ABBOUD, J.-L. M., 1991, *J. Am. chem. Soc.*, **113**, 12873.
[120] HUISGEN, R., 1977, *Accts chem. Res.*, **10**, 117.
[121] HUISGEN, R., 1980, *Pure appl. Chem.*, **52**, 2283.
[122] TRUONG, T. N., 1998, *J. Phys. Chem.*, in the press.
[123] BRESLOW, R., 1991, *Accts chem. Res.*, **24**, 159.
[124] BLAKE, J. F., and JORGENSEN, W. L., 1991, *J. Am. chem. Soc.*, **113**, 7430.
[125] CRAMER, C. J., and TRUHLAR, D. G., 1992, *J. Am. chem. Soc.*, **114**, 8794.
[126] CRAMER, C. J., and TRUHLAR, D. G., 1992, *J. comput-Aided Molec. Des.*, **6**, 629.
[127] GAJEWSKI, J. J., 1997, *Accts chem. Res.*, **30**, 219.
[128] WHITE, W. N., and WOLFARTH, E. F., 1970, *J. org. Chem.*, **35**, 2196.
[129] GUEST, J. M., CRAW, J. S., VINCENT, M. A., and HILLIER, I. H., 1997, *J. chem. Soc., Perkin Trans. II*, 71.
[130] SEHGAL, A., SHAO, L., and GAO, J., 1995, *J. Am. chem. Soc.*, **117**, 11337.
[131] SEVERANCE, D. L., and JORGENSEN, W. L., 1992, *J. Am. chem. Soc.*, **114**, 10966.
[132] STORER, J. W., GIESEN, D. J., HAWKINS, G. D., LYNCH, G. C., CRAMER, C. J., TRUHLAR, D. G., and LIOTARD, D. A., 1994, *Structure and Reactivity in Aqueous Solution*, edited by C. J. Cramer and D. G. Truhlar (Washington, DC: American Chemical Society), p. 24.
[133] STEFANOVICH, E. V., and TRUONG, T. N., 1995, *Chem. Phys. Lett.*, **244**, 65.
[134] STEFANOVICH, E. V., and TRUONG, T. N., 1996, *J. chem. Phys.*, **105**, 2961.
[135] FLORIS, F. M., TOMASI, J., and AHUIR, J. L. P., 1991, *J. comput. Chem.*, **12**, 784.
[136] JORGENSEN, W. L., and TIRADO-RIVES, J., 1988, *J. Am. chem. Soc.*, **110**, 1657.
[137] RICHARDS, F. M., 1997, *A. Rev. biophys. Bioengng*, **6**, 151.
[138] PIEROTTI, R. A., 1976, *Chem. Rev.*, **76**, 717.
[139] HURON, M. J., and CLAVERIE, P., 1972, *J. phys. Chem.*, **76**, 2123.
[140] AGUILAR, M. A., and OLIVARES DEL VALLE, F. J., 1989, *Chem. Phys.*, **138**, 327.
[141] FLORIS, F., and TOMASI, J., 1989, *J. comput. Chem.*, **10**, 616.
[142] FLORIS, F. M., TANI, A., and TOMASI, J., 1993, *Chem. Phys.*, **169**, 11.
[143] FRECER, V., MIERTUS, S., and MAJEKOVA, M., 1991, *J. molec. Struct.* (*Theochem.*), **73**, 157.
[144] OLIVARES DEL VALLE, F. J., and AGUILAR, M. A., 1993, *J. molec. Struct.* (*Theochem.*), **99**, 25.
[145] RINALDI, D., CABRAL, B. J. C., and RIVAIL, J. L., 1986, *Chem. Phys. Lett.*, **125**, 495.
[146] CAMMI, R., and TOMASI, J., 1995, *J. comput. Chem.*, **16**, 1449.
[147] KLAMT, A., and JONAS, V., 1996, *J. chem. Phys.*, **105**, 9972.
[148] LEE, B., and RICHARDS, F. M., 1971, *J. molec. Biol.*, **55**, 379.
[149] PASCUAL-AHUIR, J. L., SILLA, E., and TUÑON, I., 1994, *J. comput. Chem.*, **15**, 1127.
[150] WOON, D. E., and DUNNING JR, T. H., 1993, *J. phys. Chem.*, **98**, 1358.
[151] TRUONG, T. N., 1995, *J. chem. Phys.*, **102**, 5335.
[152] DUNCAN, W. T., and TRUONG, T. N., 1995, *J. chem. Phys.*, **103**, 9642.
[153] TRUONG, T. N., and DUNCAN, W. T., 1994, *J. chem. Phys.*, **101**, 7408.
[154] OKAMOTO, K., FUKUI, S., and SHINGU, H., 1967, *Bull. chem. Soc. Japan*, **40**, 1920.